JACC: CARDIOVASCULAR IMAGING VOL. 3, NO. 7, 2010

ISSN 1936-878X/$36.00
PUBLISHED BY ELSEVIER INC. DOI:10.1016/j.jcmg.2010.03.009

Clinical Feasibility of Accelerated, High Spatial Resolution Myocardial Perfusion Imaging

Robert Manka, MD,*† Viton Vitanis, MSc,* Peter Boesiger, PhD,*
Andreas J. Flammer, MD,‡ Sven Plein, MD, PhD,§ Sebastian Kozerke, PhD*
Zurich, Switzerland; Berlin, Germany; and Leeds, United Kingdom

OBJECTIVES The aim of this study was to assess the clinical feasibility and diagnostic performance of an acceleration technique based on *k*-space and time (*k-t*) sensitivity encoding (SENSE) for rapid, high–spatial resolution cardiac magnetic resonance (CMR) myocardial perfusion imaging.

BACKGROUND The assessment of myocardial perfusion is of crucial importance in the evaluation of patients with known or suspected coronary artery disease. CMR myocardial perfusion imaging performs favorably compared to single photon-emission computed tomography and offers higher spatial resolution, particularly when combined with scan acceleration techniques such as *k-t* SENSE. A previous study showed that *k-t* SENSE accelerated myocardial perfusion CMR with 5-fold acceleration is feasible and delivers high diagnostic accuracy for the detection of coronary artery disease. Higher acceleration factors have not been attempted clinically because of concerns over temporal blurring effects of the time-varying signal during contrast bolus passage.

METHODS Twenty patients underwent myocardial perfusion CMR imaging using a 3.0-T whole-body CMR imager before diagnostic X-ray coronary angiography. Perfusion images were obtained using an extension of the *k-t* SENSE method using parallel imaging to double the spatial resolution of the *k-t* SENSE training images. This extension, termed *k-t* SENSE+, permitted 8-fold nominal scan acceleration and an in-plane spatial resolution of up to 1.1 × 1.1 mm^2. Perfusion scores were derived by 2 blinded observers for 16 myocardial segments and compared to quantitative analysis of X-ray coronary angiography.

RESULTS CMR data were successfully obtained in all 20 patients. High diagnostic accuracy was achieved using CMR, as reflected by areas under the receiver-operator characteristic curve of 0.94 and 0.82 for detecting stenoses >50% and >75%, respectively. Observer agreement between 2 readers had a kappa value of 0.92. The areas under the receiver-operator characteristic curves for the left anterior descending, left circumflex, and right coronary artery territories with stenoses >50% were 0.75, 0.92, and 0.79, respectively.

CONCLUSIONS Accelerated CMR perfusion imaging is clinically feasible and offers excellent diagnostic performance in detecting coronary stenosis. (J Am Coll Cardiol Img 2010;3:710–7) © 2010 by the American College of Cardiology Foundation

From the *Institute for Biomedical Engineering, University and ETH Zurich, Zurich, Switzerland; †Department of Internal Medicine/Cardiology, German Heart Institute Berlin, Berlin, Germany; ‡Cardiovascular Centre, Department of Cardiology, University Hospital Zurich, Zurich, Switzerland; and the §Division of Cardiovascular and Neuronal Remodelling, University of Leeds, Leeds General Infirmary, Leeds, United Kingdom. The authors are supported by Bayer Schering Pharma AG. This work was supported by Philips Healthcare. Dr. Plein is supported by Clinical Scientist Fellowship WT078288 from the Wellcome Trust.

Manuscript received October 19, 2009; revised manuscript received March 18, 2010, accepted March 23, 2010.

The assessment of myocardial perfusion is vital in the evaluation of patients with known or suspected coronary artery disease (CAD) (1–9). Recent results from a multicenter, multivendor clinical trial have demonstrated high diagnostic accuracy of cardiac magnetic resonance (CMR) in the detection of CAD, with equal or better performance compared to single-photon emission computed tomography (10).

See page 718

In CMR perfusion imaging, spatial and temporal image resolutions must be well balanced, and they present competing constraints. With the advent of parallel imaging techniques (11,12) 2-fold scan acceleration has become feasible. In application to CMR perfusion imaging, this has enabled improved myocardial coverage without scan time penalty (13,14). Further improvements in scan efficiency have, however, been difficult to achieve as noise enhancement increases with increasing acceleration factors, severely compromising image quality.

Recognition of the importance of both high spatial and high temporal resolution in ischemia detection has fueled efforts to further advance scan acceleration methods. By exploiting the inherent similarity of images acquired at different time points during contrast bolus passage, scan acceleration factors >2 have become feasible (2,15,16). In the *k*-space and time (*k-t*) sensitivity encoding (SENSE) method (17), data correlations in space and time are used to speed up data acquisition while suppressing excessive noise amplification. The superiority of the method over parallel imaging has been demonstrated (16), with excellent diagnostic performance in detecting myocardial ischemia in a clinical population (16,18,19). With 5-fold scan acceleration, spatial resolutions of 1.3 × 1.3 mm^2 in-plane have been achieved at 3.0-T, enabling clear discrimination of subendocardial defects (19). Further progress in increasing scan efficiency has, however, been hampered by temporal blurring effects observed with increasing acceleration factors (16). This problem can partially be attributed to the low resolution of the training data used in the *k-t* SENSE method (20). To this end, an extension of *k-t* SENSE was recently presented that combines parallel imaging to boost the training data resolution without scan time penalty (21). Using this method, hereafter referred to as *k-t* SENSE+, scan accelerations >5 have been demonstrated in healthy subjects. However, clinical validation has not been performed to date.

The aim of the present study was to prospectively determine the feasibility and clinical performance of accelerated cardiac perfusion imaging using *k-t* SENSE+ for the detection of CAD, using X-ray coronary angiography as the reference standard.

METHODS

Study population. Twenty patients (16 men; mean age 60 ± 7 years; range 45 to 71 years) awaiting diagnostic invasive X-ray coronary angiography for the evaluation of known or suspected CAD were recruited consecutively between July and November 2008. All patients gave written informed consent, and the study was approved by the local ethics review board. Exclusion criteria were contraindications to CMR (mainly incompatible metallic implants and claustrophobia) or to adenosine infusion (asthma or atrioventricular block more severe than grade I), myocardial infarction within 7 days, unstable angina pectoris, and New York Heart Association functional class IV heart failure. Moreover, patients with arrhythmias and those who had undergone previous coronary artery bypass graft surgery were not considered for study inclusion. Patients were instructed to refrain from substances containing caffeine during the 24 h before the examination. Cardiac medications were not stopped before CMR.

ABBREVIATIONS AND ACRONYMS

AUC = area under the curve
CAD = coronary artery disease
CI = confidence interval
CMR = cardiac magnetic resonance
k-t = *k*-space and time
LAD = left anterior descending coronary artery
RCA = right coronary artery
ROC = receiver operator characteristic
SENSE = sensitivity encoding

CMR imaging. Patients underwent CMR imaging on a 3.0-T clinical magnetic resonance system (Philips Healthcare, Best, the Netherlands). Patients were placed in the supine position, and a 6-element cardiac phased-array coil was used for signal reception. Cardiac synchronization was performed using 4 electrodes placed on the hemithorax (vector electrocardiography), and imaging was triggered on the R-wave of the electrocardiogram (22).

After the acquisition of standard cine scans for the assessment of left ventricular function, perfusion imaging data were acquired in the short-axis orientation at 3 different cardiac levels. Adenosine was administered intravenously at a dose of 140 μg/kg/min under continuous heart rate and blood pressure monitoring at 1-min intervals. After 3 min of adenosine infusion, an intravenous bolus injection of 0.1 mmol/kg gadobutrol (Gadovist; Bayer

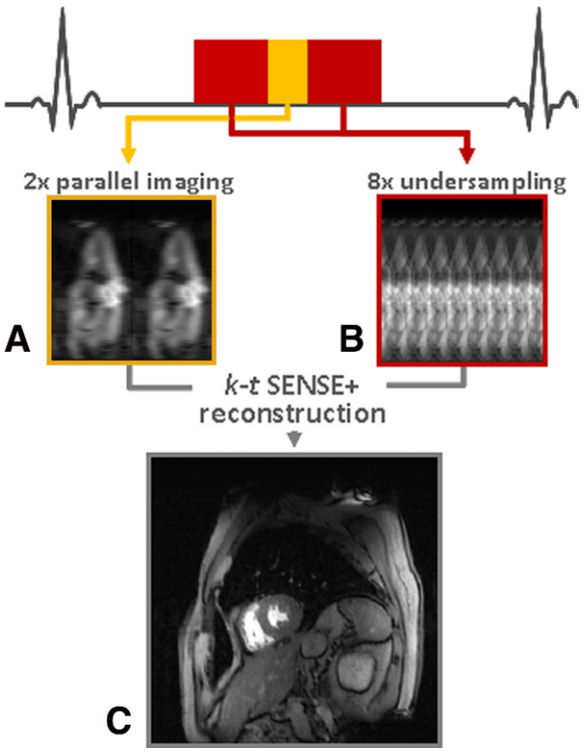

Figure 1. *k-t* SENSE+ Imaging Principle

On the basis of low-resolution training data that are acquired with 2-fold parallel imaging (**A**), an estimate of the expected signal intensities of the object is obtained and used to unfold the aliased components resulting from the 8-fold undersampled data (**B**). The high-resolution final reconstruction result (**C**). *k-t* = *k*-space and time; SENSE = sensitivity encoding.

Schering Pharma AG, Berlin, Germany) was administered into an antecubital vein on the opposing arm using a power injector (Medrad Spectris Solaris; Medrad, Indianola, Pennsylvania) at an injection rate of 5 ml/s followed by a 20-ml saline flush at 5 ml/s.

The CMR *k-t* SENSE+ perfusion imaging protocol consisted of a saturation-recovery gradient-echo pulse sequence (repetition time [TR] 2.7 ms, echo time 0.92 ms, flip angle 20°, saturation prepulse delay 150 ms, 75% partial Fourier acquisition with homodyne reconstruction, field of view 380 × 280 to 350 mm^2, slice thickness 10 mm, number of dynamics 24, end-inspiration breath-hold). The acquisition matrix was kept constant (320 × 256 profiles), resulting in an in-plane resolution of 1.1 × 1.1 to 1.4 mm^2. With 11 training profiles and an undersampling factor of 8, the net acceleration was 6.15. Accordingly, the total number of acquired profiles per slice and heartbeat amounted to 256 × 0.75/6.15 = 32, resulting in an acquisition window of 32 × TR = 87 ms. In the *k-t* SENSE+ method (21), the undersampled data are reconstructed using information from training data. Before this image reconstruction step, the training data, which are acquired at 2-fold reduction, are reconstructed using parallel imaging methods to yield a matrix consisting of 2 × 11 profiles. The schematic of the image reconstruction is shown in Figure 1.

After the perfusion protocol, late gadolinium enhanced images were acquired in short-axis orientation covering the entire left ventricle using a 3-dimensional inversion-recovery segmented *k*-space gradient-echo pulse sequence (TR 3.7 ms, echo time 1.8 ms, flip angle 15°, spatial resolution 1.5 × 1.5 × 5 mm^3).

Data analysis. All data were analyzed on a post-processing workstation (Viewforum; Philips Healthcare) by an expert observer with 4 years of experience in CMR imaging. The observer was blinded to all clinical information. For the assessment of interobserver variability, a second expert (with 8 years of experience in CMR imaging), who was equally blinded to all clinical information, independently repeated the analysis. Image quality with regard to artifacts and blurring was graded on a 4-point scale between 0 and 3 (0 = nondiagnostic, 1 = poor, 2 = good, 3 = excellent). Visual perfusion analysis used 16 segments of the American Heart Association model for left ventricular assessment (23). Perfusion in a segment was considered abnormal if 1) contrast enhancement was reduced in comparison with nonischemic myocardial segments or 2) in cases in which a transmural enhancement gradient was seen and the perfusion defect was not located within scar tissue on the corresponding late gadolinium enhanced images. Stress perfusion in each segment was scored on a 4-point scale from 0 to 3 (0 = normal, 1 = probably normal, 2 = probably abnormal or subendocardial defect, 3 = abnormal or transmural defect). A perfusion score was calculated as the sum of all segmental scores (0 to 48) for each patient. Separate perfusion scores were calculated for the left anterior descending coronary artery (LAD), left circumflex coronary artery (LCX), and right coronary artery (RCA) territories according to the American Heart Association segmentation.

To assess the value of the high spatial resolution in perfusion imaging, the acquired data were resampled to 2-fold increased voxel sizes corresponding to 4-fold increased voxel volumes by setting to zero all *k*-space samples above a cutoff frequency given by $1/(2\delta w)$, where δw denotes the in-plane voxel widths of the high-resolution data. Additional pro-

Table 1. Patient Characteristics

Variable	Value
Age (yrs ± SD)	60 ± 7
Sex, n (%)	
Male	16 (80%)
Female	4 (20%)
Risk factors and patient history, n (%)	
Hypertension	12 (60%)
Hypercholesterolemia	13 (65%)
Diabetes mellitus	6 (30%)
Smoking	8 (40%)
Family history of premature CAD	2 (10%)
Suspected CAD	9 (45%)
Known CAD	11 (55%)
Previous PCI	11 (55%)
Previous MI	4 (20%)
Angiographic findings	
No significant CAD*	10 (50%)
1-vessel disease*	8 (40%)
2-vessel disease*	2 (10%)
3-vessel disease*	0 (0%)
LAD*	4 (20%)
LCX*	3 (15%)
RCA*	5 (25%)

*Coronary artery stenosis > 50% on quantitative coronary analysis.
CAD = coronary artery disease; LAD = left anterior descending coronary artery; LCX = left circumflex coronary artery; MI = myocardial infarction; PCI = percutaneous coronary intervention; RCA = right coronary artery.

cessing, such as Hamming filtering, was not applied. Accordingly, in-plane voxel sizes of the resulting low-resolution data were 2.2 × 2.2 to 2.8 mm^2 and thus comparable with previous clinical trial studies (10). The low-resolution data were analyzed blinded to the original high-resolution data by the 2 independent observers.

Coronary angiography. Following the CMR examination, all patients underwent biplane X-ray coronary angiography using a standard technique. Angiograms were analyzed by quantitative coronary analysis (Xelera 1.2 L4 SP1; Philips Healthcare) by an independent blinded reviewer. Coronary lesions were analyzed in several projections. The severity of any coronary lesion was evaluated by measuring minimal luminal diameter and percent diameter stenosis in several angiographic views. The most severe stenosis was recorded. For analysis purposes, only vessels with reference diameters > 2 mm were included. On the basis of these analyses, patients were classified as having 1-vessel, 2-vessel, or 3-vessel disease. A significant left main coronary artery stenosis was considered double-vessel disease.

Statistical analysis. Continuous data are expressed as mean ± SD, and comparisons between groups were made by using 2-tailed paired *t* tests. No corrections were made for multiple comparisons. Discrete data are expressed as percents. Categorical data were compared by using the chi-square test. A p value <0.05 was considered to indicate a significant difference. The diagnostic accuracy of visual analysis to detect coronary stenoses with diameters more than 50% with quantitative coronary analysis of X-ray angiograms in vessels with reference diameters more than 2 mm was determined using receiver-operator characteristic (ROC) analysis (24) using MedCalc version 9.2.1.0 (MedCalc Software, Mariakerke, Belgium). The areas under the curves (AUCs) were compared using the method of DeLong et al. (25). The total perfusion score on a quantitative scale of 0 to 48 served as the analysis metric. Agreement between observers for the overall perfusion scores was assessed using the method described by Bland and Altman (26).

RESULTS

Patient characteristics and hemodynamic data. All 20 patients successfully completed CMR scans and were included in the final analysis.

Table 1 summarizes patient characteristics, and Table 2 presents hemodynamic data. X-ray coronary angiography demonstrated significant coronary artery stenoses (>50% luminal diameter reduction in vessels >2 mm in diameter) in 10 patients (50%). Eight patients (40%) had single-vessel disease and 2 patients (10%) had multivessel disease. In terms of the anatomical location of coronary artery stenoses, 4 patients (20%) had significant LAD stenoses, 3 patients (15%) had significant LCX stenoses, and 5 patients (25%) had significant RCA stenoses.

The mean heart rate showed a significant ($p < 0.0001$) increase during adenosine infusion. There were no significant changes in systolic ($p = 0.07$) or diastolic ($p = 0.81$) blood pressure. Most patients ($n = 17$) had minimal side effects (breathlessness, flushing, headache). No serious adverse events occurred.

Table 2. Hemodynamic Data at Rest and Stress

Hemodynamic Aspect	Rest	Stress
Heart rate (beats/min)	63 ± 11	81 ± 15*
Systolic blood pressure (mm Hg)	136 ± 14	134 ± 14
Diastolic blood pressure (mm Hg)	67 ± 9	67 ± 12
Pulse pressure product (beats/min × mm Hg)	8,561 ± 1,711	10,794 ± 2,422*

Data are expressed as mean ± SD. *p < 0.05.

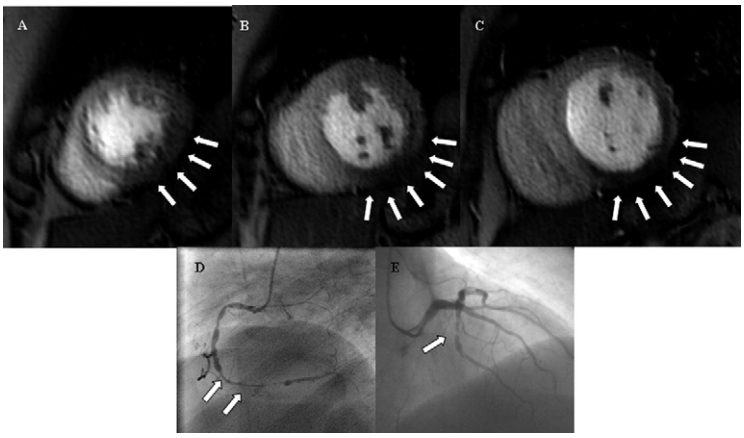

Figure 2. Case Example #1

k-Space and time (*k-t*) sensitivity encoding+ cardiac magnetic resonance perfusion images acquired during adenosine stress show a perfusion defect inferior in the apical slice **(A)** and inferior and inferolateral defects in the equatorial **(B)** and basal **(C)** slices. X-ray coronary angiography showed diffuse disease with subtotal occlusion of the right coronary artery **(D) (arrows)** and a high-degree stenosis of the left circumflex coronary artery **(E) (arrow)**.

Diagnostic accuracy. Figure 2 presents *k-t* SENSE+ perfusion images acquired during adenosine stress in a patient with suspected CAD (upper row) and the corresponding X-ray coronary angiographic images (lower row). The CMR images show an inferior perfusion defect in the apical slice and an inferior and inferolateral defect in the equatorial and basal slices. The X-ray images show a subtotal occlusion of the RCA and a high-degree stenosis of the LCX, with no significant disease in the LAD.

A second case is presented in Figure 3. The *k-t* SENSE+ perfusion images (upper row) show a circular perfusion defect in the apical slice and an anterior, anteroseptal, and inferoseptal defect in the equatorial and basal slices. The X-ray coronary angiographic images (lower row) show evidence of a high-degree stenosis in the LAD, no significant disease in the LCX, and a small, nondominant RCA.

The overall mean perfusion score was 6.2 (95% confidence interval [CI]: 3 to 10). The AUC on ROC analysis for the ability of the perfusion score

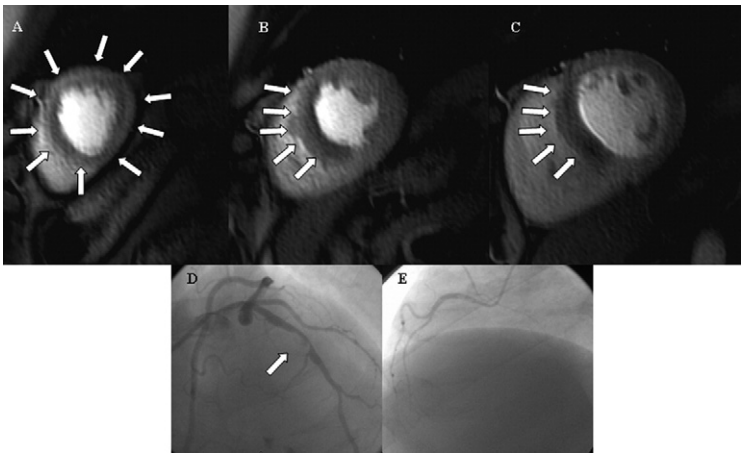

Figure 3. Case Example #2

k-Space and time (*k-t*) sensitivity encoding+ cardiac magnetic resonance perfusion images acquired during adenosine stress in a patient with suspected coronary artery disease show a circular perfusion defect in the apical slice **(A)** and anterior, anteroseptal, and inferoseptal defects in the equatorial and basal slices **(B and C)**. X-ray coronary angiography confirmed a high-degree stenosis of the left anterior descending coronary artery **(D) (arrow)** and a small right coronary artery **(E)**.

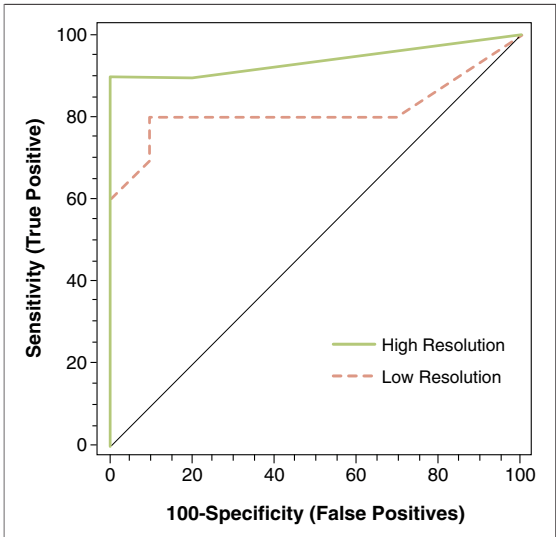

Figure 4. Receiver-Operator Characteristic Curve

Receiver-operator characteristic curve for the ability of the perfusion score to detect coronary artery disease (>50%) for high-resolution and low-resolution data. The areas under the receiver-operator characteristic curve were 0.94 for the high-resolution data and 0.82 for the low-resolution data (p = 0.13).

to detect the presence of CAD (>50%) was 0.94 (95% CI: 0.74 to 0.99) (Fig. 4). At a cutoff value of 2, this resulted in sensitivity and specificity of 90% and 100%, respectively. Using a cutoff value of 1, sensitivity and specificity were 90% and 90%, respectively. AUCs on ROC analysis were 0.75 (95% CI: 0.51 to 0.91), 0.92 (95% CI: 0.69 to 0.96), and 0.79 (95% CI: 0.55 to 0.93) for the detection of >50% coronary artery stenosis in the LAD, LCX, and RCA, respectively. The mean perfusion scores for single-vessel and double-vessel disease at disease severity >50% were 11.0 (95% CI: 5 to 17) and 16.0 (95% CI: −35 to 67), respectively. Patients without significant CAD had a mean perfusion score of 0.4 (95% CI: 0 to 1). Lower diagnostic accuracy was seen for the detection of CAD >75% (AUC: 0.82; 95% CI: 0.59 to 0.95; p = NS) compared to CAD >50%. At a cutoff value of 2, this resulted in sensitivity and specificity of 86% and 77%, respectively.

The diagnostic accuracy for the low-resolution data was not significantly different compared with that for the high-resolution data in the patient population studied: 0.82 (95% CI: 0.58 to 0.95) and 0.79 (95% CI: 0.55 to 0.94) for the detection of >50% (p = 0.13) and >75% (p = 0.72) CAD, respectively (Fig. 4). Using a cutoff value of 2, sensitivity and specificity for the detection of >50% and >75% coronary artery stenoses were 80% and 50%, and 86% and 46%, respectively.

Interobserver agreement. Agreement analysis for the overall perfusion score showed a mean bias of 0.0, with 95% limits of agreement of 3.2 to −3.2. The AUCs on ROC analysis were similar between the 2 observers for the main analysis of coronary artery stenosis >50%: 0.94 (95% CI: 0.74 to 0.99) and 0.98 (95% CI: 0.80 to 1.0) (p = 0.13).

Image quality. The mean image quality score was 2.2 ± 0.7. None of the images were considered nondiagnostic.

DISCUSSION

This study shows that accelerated CMR perfusion imaging using *k-t* SENSE+ is feasible in a clinical population, with excellent diagnostic performance to detect coronary stenosis relative to X-ray angiography.

The boundaries of CMR myocardial perfusion imaging continue to be pushed, driven by technological advances that permit faster data acquisition. This increase in speed can be invested flexibly into better spatial or temporal resolution, and both are important to maximize diagnostic performance (13,14). The latest acceleration methods, such as *k-t* SENSE, continue to evolve, and several improvements over the initial implementations have been proposed (14,18,20), each addressing particular potential limitations of the method. Defining the clinical potential of these refinements is challenging and laborious, because validation studies are required at every step of the development process. The aim of this study was to assess the clinical feasibility of *k-t* SENSE+, which allows higher acceleration than the standard *k-t* SENSE approach. In the current implementation, the increase in speed was invested in improved spatial resolution while keeping acquisition duration short. This study can only give an indication of the potential role of *k-t* SENSE+ but demonstrated that it can be applied to a consecutive clinical population and achieve high diagnostic accuracy and reproducibility.

Recent work investigating dark rim image artifacts (16,27) placed emphasis on high spatial resolution as a factor to address this issue. In the present study, spatial resolution could be increased in comparison with previous studies, preventing the appearance of such artifacts and allowing for the precise assessment of the transmural extent of the ischemic region. It is important to note that the diagnostic advantage comes at no cost with respect to the length of the acquisition window, which was kept below 90 ms/heartbeat. This has the additional

benefit of reduced intershot cardiac motion, which could otherwise result in blurring or contribute to dark rim artifacts.

With the current acceleration factors, only 3 slices could be acquired, given the shorter cycle intervals during stress exams. However, it has been indicated that even full coverage of the heart may be achieved by using additional modifications in image acquisition and reconstruction procedures. Methods based on *k-t* SENSE using temporal basis functions seem very promising in achieving acceleration factors >8 (28), but these remain to be validated clinically. Besides the advantages with respect to higher acceleration factors, these methods are also less sensitive to bulk motion of the heart in cases in which breath-holds cannot be performed. In the present study, with a small study population, all subjects could either perform the inspiration breath-holds or were asked to perform shallow expiration after an initial inspiration breath-hold, which minimizes respiration-related image artifacts seen with the *k-t* SENSE method (29).

The overall diagnostic accuracy of perfusion imaging was slightly better relative to results from a previous study by Plein et al. (19), with AUCs of 0.94 versus 0.89, respectively. Cheng et al. (5) also reported a slightly smaller AUC of 0.89 for CMR perfusion imaging at 3.0-T.

Comparison of results from high-resolution and low-resolution perfusion data revealed improved specificity at high spatial resolution. This may be explained by the reduction in subendocardial dark rim artifacts with reduced voxel sizes. Sensitivity did not differ significantly between low-resolution and high-resolution data, which is attributed to the size and composition of the present patient study population. It is speculated that sensitivity profits from higher spatial resolution primarily in patients presenting with subendocardial rather than transmural perfusion defects. In view of these issues, larger patient studies are warranted to verify the trend for higher diagnostic performance found with the *k-t* SENSE+ method.

Study limitations. A clear limitation of the present work was the limited sample size. However, taking into account previous studies using a similar method indicates overall confidence in the results obtained, which is also supported by the agreement analysis from the 2 observers evaluating data in this study. Another limitation was the use of X-ray coronary angiography to determine if relevant CAD was present, because it provides only an indirect estimate of the flow limitation caused by coronary artery stenosis. However, the modality remains the most important clinical examination to determine patient treatment.

CONCLUSIONS

In conclusion, accelerated CMR perfusion imaging using *k-t* SENSE+ is clinically feasible and offers excellent diagnostic performance in detecting CAD, as determined in this relatively small clinical population.

Acknowledgment

The authors thank Dr. Juerg Schwitter from the Department of Cardiology at the University Hospital Zurich, for expert advice and fruitful discussions on CMR perfusion imaging.

Reprint requests and correspondence: Dr. Sebastian Kozerke, Institute for Biomedical Engineering, University and ETH Zurich, Gloriastrasse 35, CH-8092 Zurich, Switzerland. *E-mail: kozerke@biomed.ee.ethz.ch.*

REFERENCES

1. Al-Saadi N, Nagel E, Gross M, et al. Noninvasive detection of myocardial ischemia from perfusion reserve based on cardiovascular magnetic resonance. Circulation 2000;101:1379–83.
2. Gebker R, Jahnke C, Paetsch I, et al. MR myocardial perfusion imaging with k-space and time broad-use linear acquisition speed-up technique: feasibility study. Radiology 2007;245:863–71.
3. Nagel E, Klein C, Paetsch I, et al. Magnetic resonance perfusion measurements for the noninvasive detection of coronary artery disease. Circulation 2003;108:432–7.
4. Schwitter J, Nanz D, Kneifel S, et al. Assessment of myocardial perfusion in coronary artery disease by magnetic resonance: a comparison with positron emission tomography and coronary angiography. Circulation 2001;103:2230–5.
5. Cheng AS, Pegg TJ, Karamitsos TD, et al. Cardiovascular magnetic resonance perfusion imaging at 3-tesla for the detection of coronary artery disease: a comparison with 1.5-tesla. J Am Coll Cardiol 2007;49:2440–9.
6. Ingkanisorn WP, Kwong RY, Bohme NS, et al. Prognosis of negative adenosine stress magnetic resonance in patients presenting to an emergency department with chest pain. J Am Coll Cardiol 2006;47:1427–32.
7. Klem I, Greulich S, Heitner JF, et al. Value of cardiovascular magnetic resonance stress perfusion testing for the detection of coronary artery disease in women. J Am Coll Cardiol Img 2008;1:436–45.
8. Klem I, Heitner JF, Shah DJ, et al. Improved detection of coronary artery disease by stress perfusion cardiovascular magnetic resonance with the use of delayed enhancement infarction imaging. J Am Coll Cardiol 2006;47:1630–8.

9. Klein C, Nagel E, Gebker R, et al. Magnetic resonance adenosine perfusion imaging in patients after coronary artery bypass graft surgery. J Am Coll Cardiol Img 2009;2:437–45.
10. Schwitter J, Wacker CM, van Rossum AC, et al. MR-IMPACT: comparison of perfusion-cardiac magnetic resonance with single-photon emission computed tomography for the detection of coronary artery disease in a multicentre, multivendor, randomized trial. Eur Heart J 2008;29:480–9.
11. Pruessmann KP, Weiger M, Scheidegger MB, Boesiger P. SENSE: sensitivity encoding for fast MRI. Magn Reson Med 1999;42:952–62.
12. Sodickson DK, Manning WJ. Simultaneous acquisition of spatial harmonics (SMASH): fast imaging with radiofrequency coil arrays. Magn Reson Med 1997;38:591–603.
13. Kellman P, Derbyshire JA, Agyeman KO, McVeigh ER, Arai AE. Extended coverage first-pass perfusion imaging using slice-interleaved TSENSE. Magn Reson Med 2004; 51:200–4.
14. Plein S, Radjenovic A, Ridgway JP, et al. Coronary artery disease: myocardial perfusion MR imaging with sensitivity encoding versus conventional angiography. Radiology 2005;235:423–30.
15. Adluru G, Awate SP, Tasdizen T, Whitaker RT, Dibella EV. Temporally constrained reconstruction of dynamic cardiac perfusion MRI. Magn Reson Med 2007;57:1027–36.
16. Plein S, Ryf S, Schwitter J, Radjenovic A, Boesiger P, Kozerke S. Dynamic contrast-enhanced myocardial perfusion MRI accelerated with k-t sense. Magn Reson Med 2007;58:777–85.
17. Tsao J, Boesiger P, Pruessmann KP. k-t BLAST and k-t SENSE: dynamic MRI with high frame rate exploiting spatiotemporal correlations. Magn Reson Med 2003;50:1031–42.
18. Kozerke S, Plein S. Accelerated CMR using zonal, parallel and prior knowledge driven imaging methods. J Cardiovasc Magn Reson 2008;10:29.
19. Plein S, Schwitter J, Suerder D, Greenwood JP, Boesiger P, Kozerke S. k-Space and time sensitivity encoding-accelerated myocardial perfusion MR imaging at 3.0 T: comparison with 1.5 T. Radiology 2008;249: 493–500.
20. Hansen MS, Kozerke S, Pruessmann KP, Boesiger P, Pedersen EM, Tsao J. On the influence of training data quality in k-t BLAST reconstruction. Magn Reson Med 2004;52:1175–83.
21. Vitanis V, Manka R, Boesiger P, Kozerke S. Accelerated cardiac perfusion imaging using k-t SENSE with SENSE training. Magn Reson Med 2009;62:955–65.
22. Fischer SE, Wickline SA, Lorenz CH. Novel real-time R-wave detection algorithm based on the vectorcardiogram for accurate gated magnetic resonance acquisitions. Magn Reson Med 1999;42:361–70.
23. Cerqueira MD, Weissman NJ, Dilsizian V, et al. Standardized myocardial segmentation and nomenclature for tomographic imaging of the heart: a statement for healthcare professionals from the Cardiac Imaging Committee of the Council on Clinical Cardiology of the American Heart Association. Circulation 2002;105:539–42.
24. Swets JA. Measuring the accuracy of diagnostic systems. Science 1988;240: 1285–93.
25. DeLong ER, DeLong DM, Clarke-Pearson DL. Comparing the areas under two or more correlated receiver operating characteristic curves: a nonparametric approach. Biometrics 1988;44:837–45.
26. Bland JM, Altman DG. Statistical methods for assessing agreement between two methods of clinical measurement. Lancet 1986;1:307–10.
27. Di Bella EV, Parker DL, Sinusas AJ. On the dark rim artifact in dynamic contrast-enhanced MRI myocardial perfusion studies. Magn Reson Med 2005;54:1295–9.
28. Pedersen H, Kelle S, Ringgaard S, et al. Quantification of myocardial perfusion using free-breathing MRI and prospective slice tracking. Magn Reson Med 2009;61:734–8.
29. Plein S, Kozerke S, Suerder D, et al. High spatial resolution myocardial perfusion cardiac magnetic resonance for the detection of coronary artery disease. Eur Heart J 2008;29:2148–55.

Key Words: coronary artery disease ■ ischemia ■ cardiac magnetic resonance ■ myocardial perfusion ■ *k-t* SENSE.